# Observation of Oscillatory Resistance Behavior in Coupled Bernal and Rhombohedral Stacking Graphene

**Yanping Liu,[†] Wen Siang Lew,[†,*] Sarjoosing Goolaup,[†] Hwi Fen Liew,[†] Seng Kai Wong,[‡] and Tiejun Zhou[‡]**

[†]School of Physical and Mathematical Sciences, Nanyang Technological University, 21 Nanyang Link, Singapore 637371 and [‡]Data Storage Institute, Agency for Science, Technology and Research (A*STAR), DSI Building, 5 Engineering Drive 1, Singapore 117608

**ABSTRACT** We report on the first observation of an anomalous temperature-dependent resistance behavior in coupled Bernal and rhombohedral stacking graphene. At low-temperature regime (<50 K) the temperature-dependent resistance exhibits a drop while at high-temperature regions (>250 K), the resistance increases. In the transition region (50–250 K) an oscillatory resistance behavior was observed. This property is not present in any layered graphene structures other than five-layer. We propose that the temperature-dependent resistance behavior is governed by the interplay of the Coulomb and short-range scatterings. The origin of the oscillatory resistance behavior is the ABCAB and ABABA stacking configurations, which induces tunable bandgap in the five-layer graphene. The obtained results also indicate that a perpendicular magnetic field opens an excitonic gap because of the Coulomb interaction-driven electronic instabilities, and the bandgap of the five-layer graphene is thermally activated. Potentially, the observed phenomenon provides important transport information to the design of few-layer graphene transistors that can be manipulated by a magnetic field.

**KEYWORDS:** graphene · oscillatory resistance · Coulomb interaction · short-range scattering · Bernal and rhombohedral stacking · excitonic gap · thermally activated

Graphene, a newly discovered two–dimensional monolayer carbon material, has attracted intense attention recently because its unique electronic transport properties have shown remarkable application potential in nanoelectronic devices.[1–4] The low-energy quasi-particles of graphene are found to be chiral and massless Dirac fermions, which contributes to many exciting properties; such as the anomalous quantum hall effect.[5–11] The electronic transport properties of graphene can be controlled by the application of external electric or magnetic fields, or *via* the setup of graphene topology, that is, zigzag or armchair configurations.[12–14] When two monolayer graphenes are stacked together, they form the so-called bilayer graphene, which has a quadratic low-energy band structure. Bilayer graphene is reported to exhibit tunable bandgap[15,16] and giant intrinsic carrier mobility,[17] which are close to semiconductor properties. The focus of graphene study is gradually extending to structures with higher numbers of layers or few-layer graphene (FLG). A number of experimental and theoretical analyses have shown that FLG possesses features that are different from that of monolayer and bilayer graphene.[18,19] Three to five layer graphene is the subject of considerable interest, as the layer stacking configurations complicate the electronic interactions.[20,21] Trilayer graphene has a complex band structure where it contains a combination of two near-linear and four parabolic conduction bands, the former is similar to that of monolayer while the latter is similar to that of bilayer graphene.[22,23] A gate-tunable overlap bandgap in trilayer graphene was subsequently reported which leads to the conclusion that it is a semimetal.[24] Nonetheless, the theoretical understanding and experimental study of FLG is still not as established as that of monolayer and bilayer graphene. The influence of layer stacking onto the band structure and transport properties still require further experimental investigations.

In this letter we report on the electronic and magneto-transport properties of mechanically exfoliated five-layer graphene. An anomalous temperature-dependent resistance was observed. The resistance behavior was characterized by three distinct regions. Below 50 K, the resistance decreases linearly under the influence of Coulomb scattering; while above 250 K, the short-range scattering is dominant, leading to a linear increase with temperature. However, between these two temperature ranges the measured resistance oscillates with increasing trend. This is attributed to the transition from the Coulomb to the short-range scattering. Two different stacking configurations in the five-layer graphene contribute to the oscillatory resistance property. These properties have not been observed in any graphene structures.

* Address correspondence to wensiang@ntu.edu.sg.

Received for review February 24, 2011 and accepted June 25, 2011.

**Published online June 25, 2011**
**10.1021/nn200771e**

Perpendicular magnetic field induces an excitonic bandgap, leading to a lower conductivity. The obtained results are important for the illustrated fact that measurement magnetic field dependence of resistance for these electron densities is used as a qualitative proof for the opening of an energy gap.

## RESULTS AND DISCUSSION

To identify and confirm the layer precision of our graphene sample, we have carried out contrast spectra measurement of different layers of graphene samples. As shown in Figure 1a, the contrast spectra provides a quantitative guide to the visual confirmation of graphene layers.[25−28] To ascertain that our sample structure is a five layer graphene, micro-Raman spectroscopy measurement was employed *via* the 2D-band deconvolution procedure.[29−31] The inset of Figure 1a, clearly depicts the G and 2D band of the respective graphene layers. Additionally, we have also used AFM to measure the thickness of five-layer graphene. The AFM image and height profiles of the five-layer graphene are shown in Figure 1b. The height of the graphene sample is 2.155 nm which is slightly larger than the theoretical value of (0.334 nm × 5 = 1.670 nm). This difference is attributed to a "dead" space between the graphene sample and $SiO_2$ substrates.[3,4]

Shown in Figure 2a is the current−voltage (*I*−*V*) relationship of five-layer graphene at different temperatures and magnetic fields. The magnetic field was applied perpendicularly to the plane of the graphene. Also shown in the inset is an optical micrograph of a typical four-terminal configuration that is used for the transport measurement. The linear *I*−*V* relationship indicates that the five-layer graphene behaves as a linear resistor in nature. The increase in resistance as the temperature is reduced is typical of an intrinsic semiconductor property. On the other hand, for a fixed temperature, the resistance increases with increasing perpendicular magnetic field. Such a behavior indicates that an opening of the energy gap due to the application of perpendicular magnetic fields has caused resistance increase. The four-terminal magnetoresistance measurements of the five-layer graphene for temperatures 2−50 K is shown in Figure 2b. The measured resistance is plotted as resistance per square, so that it is independent of the sample size. For temperature lower than 20 K, the measured resistance drops quickly when a relatively small field (0.2 T) is applied. As the temperature increases the drastic phenomena of magnetoresistance is diminishing. This is the characteristic of weak localization effect, which originates from the intervalley scattering because of atomically sharp scatters in a realistic graphene sheet.[32−35] The suppression of the weak localization property is mainly dependent on the

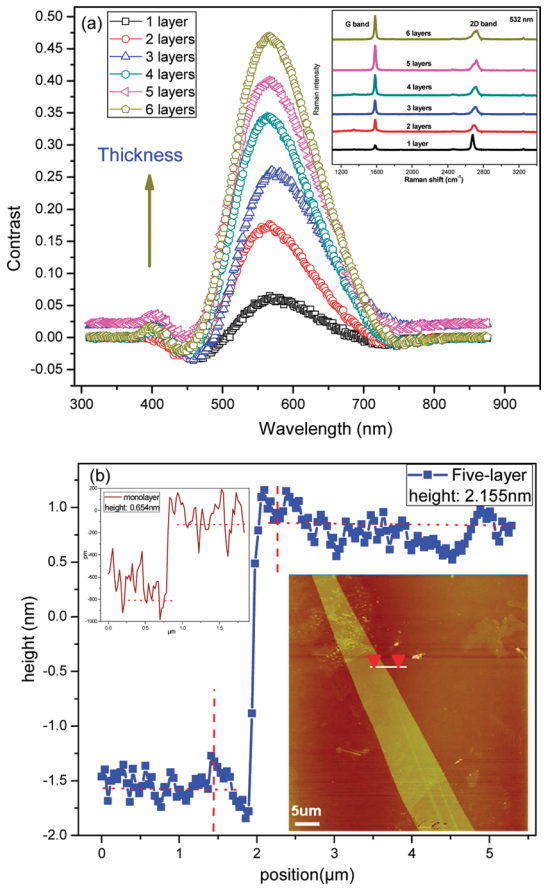


**Figure 1. (a) Contrast spectrum measurement of graphene. Inset shows comparison of Raman spectra at 532 nm for mono- to six-layer graphene. The position of G peak and the spectral features of 2D band indicate the number of graphene layer. (b) AFM height profiles indicated by the red box in the inset AFM topographic image of five-layer graphene. Inset show the height profiles of monolayer graphene. Scale bar represents 5 $\mu$m.The height of monolayer and five-layer is 0.654 nm and 2.155 nm, respectively.**

trigonal warping of the graphene bands,[36−38] resulting in an asymmetry of the carrier dispersion with respect to the center of the corresponding valley. This is the first observation of a weak localization effect in five-layer graphene, and our systematic multilayer graphene investigations reveal that the weak localization effect becomes more pronounced when the number of graphene layers is increased from two to five.[23] Figure 2c shows a close-up view of the resistance transition region at low temperatures where the weak localization effect is significant.

In FLGs, each Landau level at energy $E_n$ is assumed to be 4-fold degenerate due to 2-fold spin degeneracy and 2-fold sublattice symmetry. The application of a magnetic field induces sublattice symmetry breaking, and the gap formation is caused by many-body correction in the Landau level.[39,40] The gap as shown in Figure 3a, is excitonic in nature and increases with $\sqrt{\mathbf{B}}$. The four-terminal resistance measurements of five-layer graphene at large magnetic field, in the

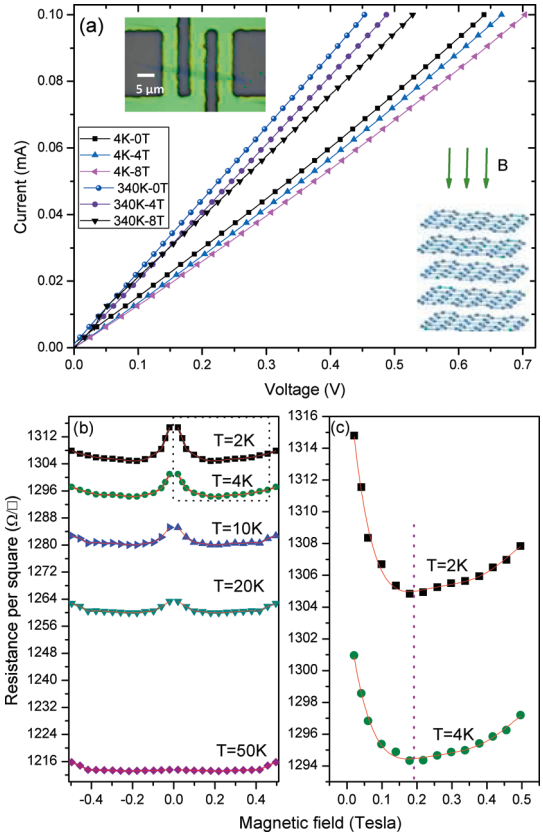


**Figure 2. (a) Current−voltage characteristics of five-layer graphene at temperatures 4 and 340 K. The measurements show an Ohmic behavior irrespective of the presence of an applied magnetic field. Top corner inset is an optical micrograph of our graphene four-terminal configuration. Bottom corner inset shows contrast spectra measurements of one to six layers of graphene structures, the number of graphene layers in our samples can be precisely determined *via* this optical measurement method. (b). Four-terminal resistance measurement of five-layer graphene as a function of magnetic field at different temperatures. At low temperatures the resistance drops quickly when a relatively small perpendicular field is applied; it increases slightly before saturation when the field strength is further enhanced. This phenomenon is gradually diminishing when the measurement temperature is increased from 2 to 20 K and completely disappears at 50 K. This observation indicates the presence of a weak localization effect in five-layer graphene. (c) A close-up view of the resistance transition region at low temperatures where the weak localization effect is significant.**

temperature range of 4−340 K is shown in Figure 3b. The measurements reveal that the longitudinal resistance $R_{xx}$ has a nonlinear relationship with magnetic field strength. It is in contradiction with the Zeeman spin-splitting model, where the Zeeman spin-splitting gap is given by

$$\Delta_z = g\mu_B \mathbf{B} \quad (1)$$

where $g$ is the free-electron $g$-factor $g = 2$ and $\mu_B$ is the Bohr magneton.[41] The origin of the smooth resistance increment is the splitting of Landau level that gives rise to a bandgap opening at zero energy level.[39,42] This is ascribed to the attractive interaction between electron−hole pairs that forms a condensation gap when Coulomb interaction is included. The dotted line in Figure 3b is a fit following the relationship

$$R_{xx} \sim \exp[-\Delta E/k_B T] \quad (2)$$

where $k_B$ is the Boltzmann constant, and $\Delta E$ is the energy gap.[41,42] As $\Delta E$ is proportional to $\sqrt{\mathbf{B}}$, we can rewrite that as

$$R_{xx} \propto \exp(\sqrt{\mathbf{B}}/k_B T) \quad (3)$$

This equation is in good agreement with our experimental data. This behavior differs from that of monolayer and bilayer graphene, where the resistance increases nonlinearly with magnetic field strength and exhibits plateau-like phases. As such, our results reveal that the additional layer in five layer graphene as compared to mono and bilayer graphene significantly screens the ripple effect.

One should note that weak localization is not the origin of the positive magnetoresistance as seen in Figure 2b. A possible mechanism for the positive magnetoresistance in the five-layer graphene sample is charge inhomogeneity.[43] The conductivity around the charge neutral point, dominated by charge disorder, creates electron and hole puddles in the sample.[44] Within the Drude model, a conductor with electrons and holes may show large transverse magnetoresistance, due to the electrons and holes developing components of drift velocity perpendicular to the current, giving rise to zero net transverse current. Both holes and electrons are present at finite temperatures in graphene. Such a two-fluid system having equal mobility for both types of carriers, can yield positive magnetoresistance due

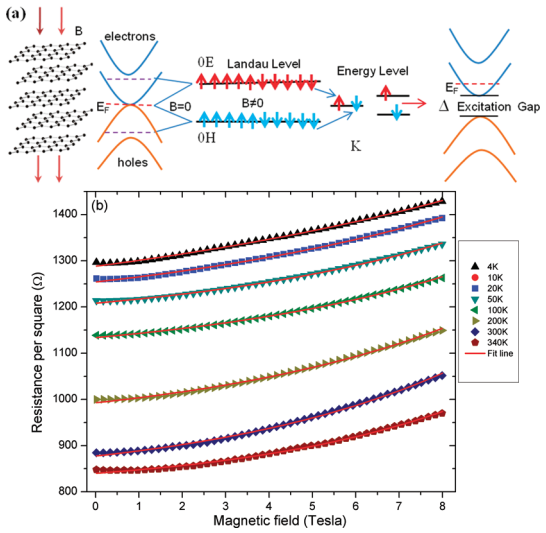


**Figure 3. (a) Illustration of the five-layer graphene bandgap and Landau level splitting under the application of a magnetic field. The zero-energy state with respect to up-spin electrons and down-spin holes make an excitation condensation gap due to the attractive Coulomb force between a hole and an electron. (b) Resistance measurement with a larger magnetic field range of the five-layer graphene at different temperatures. The results show that the magnetoresistance nonlinear increase with magnetic field strength at the different temperature. The line is fits following the relationship $R_{xx} \propto \exp(\sqrt{B}/k_B T)$.**

to a net drift velocity perpendicular to the applied current at finite magnetic field.[43,45]

The resistance of the charge carrier in graphene is greatly influenced by scattering mechanisms. The main scattering mechanisms in FLG are Coulomb scattering,[46] short-range scattering[45] and phonon scattering by graphene phonon.[47] These scattering mechanisms are strongly dependent on temperature. To understand the effect of crystallographic stacking orders on the scattering mechanisms, we have carried out a systematic study of the transport properties of pure ABABA and ABCAB graphene structure. In Figure 4a,c,e, we present the normalized resistance $R_T/R_{T=340K}$ of the two different crystallographic stacking orders in five-layer graphene as a function of temperature, under the conditions of zero and 12 T magnetic fields. The measured resistance decreases monotonically as the temperature is increased from 2 to 340 K, irrespective of the magnetic field strength. The higher resistance observed confirms the opening of an excitonic energy gap in the five-layer graphene when a perpendicular field of 12 T is applied. The temperature dependence of mobility in five-layer graphene is mainly determined by Coulomb and short-range scatterings, which are caused by the source of impurities and defects, respectively. To deduce the five-layer graphene mobility, we first assume that the scattering charge centers are at the $SiO_2$—graphene interface and the short-range scattering is a constant.[48] The transport scattering rate can be written as

$$\frac{1}{\tau(\mathbf{E}_k)} = \frac{2\pi n_i}{\hbar}\int_{k'}\frac{d^2k'}{(2\pi)^2}\left|\frac{V(q)}{\varepsilon(q)}\right|^2 \times(1+\cos\theta_{kk'})(1-\cos\theta_{kk'})\,\delta(\mathbf{E}_k-\mathbf{E}_{k'}) \quad (4)$$

according to the Fermi-Golden rule, where $V(q)$ is the matrix element of the scattering potential, $\theta_{kk'}$ is the angle between the scattering in and out wave vector $k$ and $k'$, $\varepsilon(q)$ is the 2D finite temperature static random-phase-approximation dielectric function appreciate for graphene, $n_i$ is the concentration of the impurity center. The energy average scattering time can be expressed as[48]

$$\langle\tau\rangle = \int d\mathbf{E}_k\,\mathbf{E}_k\tau(\mathbf{E}_k)\left(-\frac{\partial f}{\partial \mathbf{E}_K}\right)\Big/\int d\mathbf{E}_k\,\mathbf{E}_k\left(-\frac{\partial f}{\partial \mathbf{E}_K}\right) \quad (5)$$

where $\mathbf{E}_k$ is the wave vector energy, $\tau(\mathbf{E}_k)$ is the transport scattering rate. The density-of-states function in five-layer graphene is a constant:

$$D(E_F) = \frac{2m^*}{\pi\hbar^2} \quad (6)$$

where the Fermi energy is $E_F = \hbar^2k^2/2m^* = \hbar^2\pi n/2m^*$. From the Boltzmann equation of mobility:

$$\mu = \frac{eD(E_F)v_F{}^2(\tau)}{2n} \quad (7)$$

we can obtain the mobility of five-layer graphene as

$$\mu_{5\,\text{layers}} = \frac{e\langle\tau\rangle}{m^*} \quad (8)$$

By using the Matthiessen's rule the overall mobility can be expressed as[45]

$$\mu_{\text{total}}{}^{-1} = \mu_C{}^{-1} + \mu_{SR}{}^{-1} \quad (9)$$

where $\mu_C$, $\mu_{SR}$ are the mobility of Coulomb scattering and short-range scattering, respectively. It has been shown by Zhu et al.[48] that the Coulomb scattering is a strong function of temperature,

$$\mu_{5\,\text{layers}} \propto k_B T \quad (10)$$

and the short-range scattering is independent of charge density in FLG. With that deduction, we can use the following expression to fit the measured resistance for five-layer graphene:

$$R_{5\,\text{layers}} = R_{\text{C-5 layers}} + R_{\text{SR-5 layers}} \quad (11)$$

where we find $R_{\text{C-5 layers}} = 1/((a+bT)\cdot ne)$, $R_{\text{SR-5 layers}} = c$, and $a$, $b$, and $c$ are the fitting parameters. The model fits well with the obtained measurements as shown in Figure 4a,c,e. The value of the short-range scattering parameter has increased when the five-layer graphene is subjected to a magnetic field, indicating the influence of external magnetic field on lattice defects.[49−51] These considerations explain qualitatively why the

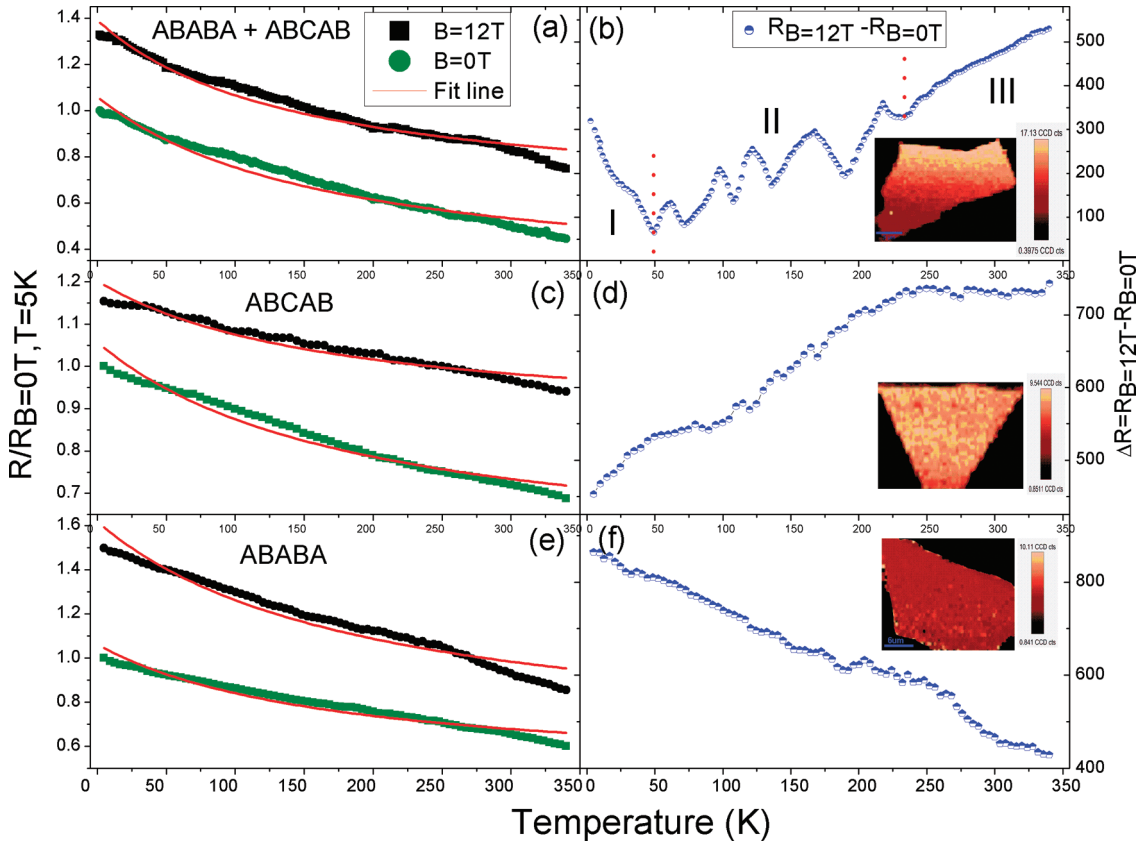


**Figure 4. (a, c, and e) The relative change of resistance per square measurements of the five-layer graphene as a function of temperature at different magnetic fields with different crystallographic stacking orders. The measurements show that when the temperature increases from 4 to 340 K, the resistance of the five-layer graphene drops significantly. This result indicates that an intrinsic semiconductor property is present and an applied perpendicular magnetic field could induce high resistance. The symbols are the measured data and the lines are fits. (b, d, and f) Four-terminal resistance of the five-layer graphene $R_{B=12T} - R_{B=0T}$ as a function of temperature with different crystallographic stacking orders.. The results of mixed stacking orders indicate that the relative resistance values change at three different temperature regimes. (b) Region I is under the influence of the Coulomb scattering. Region III is dominated by the short-range scattering. The oscillatory resistance in region II is due to the competition of the Coulomb and the short-range scattering. (d) For the ABCAB stacking, the results show that the relative resistance values rise with the increasing temperature. This indicates that a magnetic field opens an excitonic gap because of the Coulomb interaction-driven electronic instabilities. (f) For the ABABA stacking, the results show that the relative resistance value decreases with the increasing temperature which exhibit stability with semimetallic property. Inset shows the Raman 2D-mode spectra of the five-layer graphene with ABCAB and ABABA stacking orders. The red and yellow regions in the images correspond, respectively, to ABABA and ABCAB five-layer graphene domains. The scale bars are 3 $\mu$m in length.**

resistance of five-layer graphene decreases with increasing temperature. This is further evidenced by the increase in resistance as the magnetic field is increased.

We plot the relative change in resistance, $\Delta R = R_{B=12T} - R_{B=0T}$ as a function of temperature in Figure 4b,d,f. As shown in Figure 4b,d f, the results indicate that the relative resistance dependence on temperature between the ABCAB flake and ABABA flake is qualitatively different. We argue that this remarkable relative resistance dependence on temperature originates from different crystallographic stacking orders in the five-layer graphene, which strongly influence their electronics properties.[51−53] The bandstructure is dependent on the stacking and the perpendicular field in layered graphene.[18] Recent studies[18,53−55] have shown that the stacking of Bernal (ABA) graphene samples exhibit stability with semimetallic property, while rhombohedral (ABC) graphene samples show tunable band gap as induced by a perpendicular electric field. Rui et al.[56] have reported that the line shape and width of the Raman 2D mode provides a useful tool for identification the characterization of stacking order with respect to the Bernal and rhombohedral in FLG. The inset of Figure 4b,d,f shows the Raman 2D-mode spectra of the five-layer graphene used in our experiment. The ABCAB and ABABA stacking orders are clearly distinguished in our graphene sample. The red and yellow regions in the images correspond, respectively, to ABABA and ABCAB five-layer graphene domains. For the ABCAB stacking, the results show that the relative resistance value rises with the increasing temperature. The presence of the pure ABCAB stacking in our sample implies that the bandgap of the five layer graphene is opened by the presence of the external

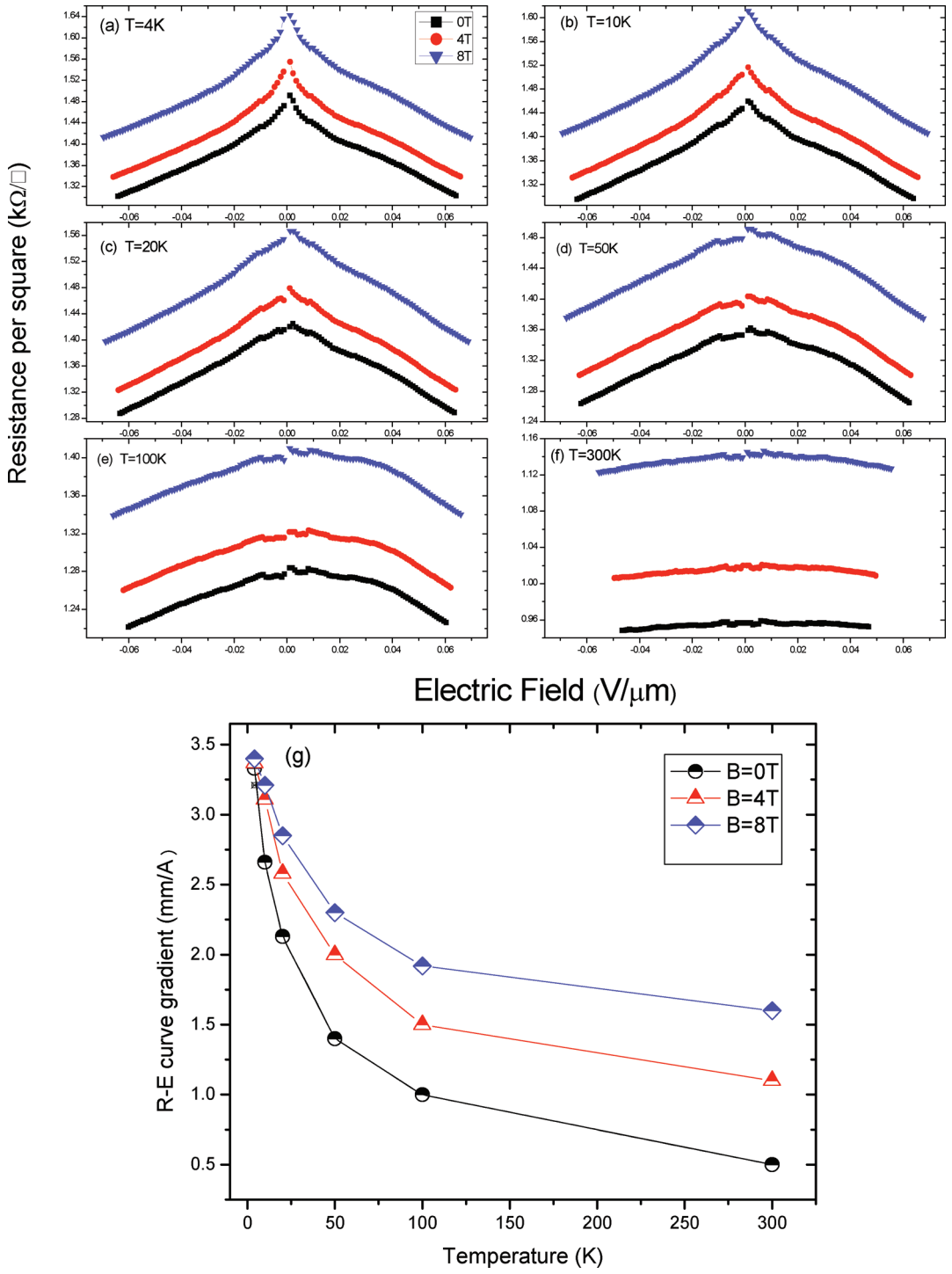


**Figure 5. (a–f) Resistance measurements as a function of electric field in five-layer graphene under different perpendicular magnetic fields and temperatures. (g) Gradient of the *R–E* curve as a function of the temperature. As the temperature increases the dependence of the measured resistance on electric field is gradually weaken because the scattering induced by electric field from the substrate surface polar phonons is significantly screened by the additional layer at room temperature.**

magnetic field. Under the applied perpendicular magnetic field, our result indicates that a magnetic field opens an excitonic gap because of the Coulomb interaction-driven electronic instabilities and the bandgap of the five layer graphene is thermally activated. So the bandgap is strongly dependent on the temperature under the application of magnetic field, namely, on the Fermi level near the five-layer graphene band structure. For the pure ABABA stacking, the results show that the relative resistance values decreases with increasing temperature, exhibiting semimetallic property. However, for the mixed ABABA and ABCAB stacking sample, the relative resistance of the five-layer graphene exhibits an oscillatory behavior as a function of increasing

temperature. This oscillation behavior originates from different bandgaps which are induced by different crystallographic stacking orders under the application of amagnetic field in the five-layer graphene.[51−53] Therefore, experimental challenges for the fabrication of these different stacked of FLGS would be very interesting.

This relative oscillatory resistance dependence on temperature properties implies that the five-layer graphene energy bandgap is a function of both the magnetic field and temperature, *i.e.*, $\Delta E$ (**B**, *T*). For lower temperature range, that is, region I ($T < 50$ K), the dominant scattering mechanism is impurity Coulomb scattering, hence the relative resistance follows the relationship $R_{xx} \propto \exp[\Delta E/k_B T]$. For higher temperatures ($T > 250$ K), the relative resistance shows a linear relationship. This is caused by the defect short-range scattering which dominates at high temperature. For the temperature range 50 K< $T < 250$ K, the resistance increases with an oscillating property. The observed oscillatory behavior is due to the competition between the two dominant modes of scattering.

Graphene is a natural charge carrier system with both neutral and charge impurities. These impurities in graphene can act as additional sources of scattering center and produce variation of the crystal potential. The short-range scattering due to defects and dislocation in graphene lattice induces a short-range potential. This potential result in a small additional resistivity which is constant and independent of the induced carrier concentration.[45,48] However, the coulomb scattering originating from charge impurities, induces long-range Coulomb potential and leads to the resistance being proportional to temperature.[46,48] In such a two-type charge carrier system, the combined total scattering time contributes to the graphene conductivity. The Coulomb scattering time is proportional to the charge impurities concentration $\tau_C \propto (n_i)^{1/2}$, while the short-range scattering time is inversely proportional to the neutral impurities concentration $\tau_s \propto (1)/((n_p)^{1/2})$. From that it is clear that the Coulomb scattering dominates at lower temperature, while short-range scattering has more influence at higher temperature. The competition between these two types of scatterers determines the conductivity of graphene in different charge concentration regimes *n*. However, the carrier density of FLG is proportional to the increasing temperature.[48] Different scattering mechanisms dominate at different temperatures. The crossover between these two mechanisms occurs in the temperature region where the two scattering potentials are equivalent. In our results, the crossover temperature regime was in the range of 50−250 K.

Figure 5 panels a−f show the resistance of the five-layer graphene as a function of an electric field under different magnetic field strengths and temperatures. The measured *R*−*E* curves are nearly symmetric when the applied electric fields sweep from positive to negative values because of the chirality of graphene electrons. As the temperature increases the rate of the resistance drop or the gradient of the *R*−*E* curve is decreasing, as plotted in Figure 5g. The larger resistance drop at lower temperature range, specifically for $T < 50$ K, indicates that Coulomb scattering is the main scattering mechanism in the five-layer graphene within this temperature range. As the Coulomb scattering time is proportional to the carrier density $n_{Dirac} \propto k_B T$,[48] it is a strong function of temperature. The dependence of the measured resistance on electric field indicates that the scattering induced by electric field from the substrate surface polar phonons is significantly screened at room temperature.[57] The application of magnetic field that has caused the increase of resistance is similar to our previous explanation.

## CONCLUSIONS

In conclusion, we have investigated the temperature and magnetic field dependence of electrical resistance in five-layer graphene. The transport measurements have revealed that the relative change of resistance as induced by perpendicular magnetic fields is thermally activated. This relative oscillatory resistance dependent on temperature properties originates from different bandgap which are induced by different crystallographic stacking orders (ABCAB and ABABA) under the application of a magnetic field in the five-layer graphene. The measured resistance increases nonlinearly with magnetic field which implies sublattice symmetry breaking and gap formation due to many-body correction in the Landau level. As the temperature-dependent resistance behavior is a good indicator of the five-layer graphene bandgap the observed relative resistance oscillation infers the thermally activated behavior. By using a combination of the Coulomb and short-range scattering mechanisms, an analytical model was used to explain the results. Additionally, the dependence of the measured resistance on electric field indicates that the scattering induced by electric field from the substrate surface polar phonons is significantly screened at room temperature.

## EXPERIMENTAL METHODS

The graphene layers are produced using mechanical exfoliation techniques[2] from the bulk highly oriented pyrolitic graphite (grade ZYA, SPI Supplies) on $Si/SiO_2$ (300 nm) substrates. Optical microscopy was used to locate the graphene flakes. One to five layers graphene samples were confirmed by Raman and contrast spectroscopy with WITEC CRM200 Raman system under 532 nm excitation wavelength in the backscattering configuration and using a 100× objective lens with a numerical aperture (NA) of 0.95[28]. The graphene contact electrodes are fabricated using

photolithography techniques. Cr (10 nm)/Au (90 nm) contact electrodes were deposited *via* thermal evaporation techniques at $10^{-7}$ mbar conditions. The patterns were obtained after lift-off in warm acetone. Electronic transport measurements were carried out on multiple samples, using PPMS (Quantum Design) with a fixed excitation current of 0.01 mA. For magnetic field measurement, the field was applied along the perpendicular direction to the plane of the sample. Thermal annealing was carried out above 300 °C in vacuum being 3 h in duration. *In situ* sample cleaning by magnetic and electric fields were performed to improve the transport measurements. Four-terminal electrical measurements were used for transport characterization.

*Acknowledgment.* This work was supported in part by the NRF-CRP program (Multifunctional Spintronic Materials and Devices) and the Agency for Science, Technology and Research (A*STAR) SERC grant (082 101 0015). The authors acknowledge Cheong Siew Ann (NTU) for useful discussions. The authors also thank Sun Li, Zhang Mingsheng (A*STAR) and Li Yuanqing for their assistance in experimental measurements.

## REFERENCES AND NOTES

1. Geim, A. K.; Novoselov, K. S. The Rise of Graphene. *Nat. Mater.* **2007**, *6*, 183–91.
2. Novoselov, K. S.; Geim, A. K.; Morozov, S. V.; Jiang, D.; Katsnelson, M. I.; Grigorieva, I. M.; Dubonos, S. V.; Firsov, A. A. Two-dimensional Gas of Massless Dirac Fermions in Graphene. *Nature* **2005**, *438*, 197–200.
3. Novoselov, K. S.; Geim, A. K.; Morozov, S. V.; Jiang, D.; Zhang, Y.; Dubonos, S. V.; Grigorieva, I. V.; Firsov, A. A. Electric Field Effect in Atomically Thin Carbon Films. *Science* **2004**, *306*, 666–9.
4. Novoselov, K. S.; Jiang, D.; Schedin, F.; Booth, T. J.; Khotkevich, V. V.; Morozov, S. V.; Geim, A. K. Two-Dimensional Atomic Crystals. *Proc. Natl. Acad. Sci. U.S.A.* **2005**, *102*, 10451–3.
5. Novoselov, K. S.; Jiang, Z.; Zhang, Y.; Morozov, S. V.; Stormer, H. L.; Zeitler, U.; Maan, J. C.; Boebinger, G. S.; Kim, P.; Geim, A. K. Room-Temperature Quantum Hall Effect in Graphene. *Science* **2007**, 1137201.
6. Semenoff, G. W. Condensed-Matter Simulation of a Three-Dimensional Anomaly. *Phys. Rev. Lett.* **1984**, *53*, 2449.
7. Geim, A. K. Graphene: Status and Prospects. *Science* **2009**, *324*, 1530–4.
8. Kim, K. S.; Zhao, Y.; Jang, H.; Lee, S. Y.; Kim, J. M.; Ahn, J. H.; Kim, P.; Choi, J. Y.; Hong, B. H. Large-Scale Pattern Growth of Graphene Films for Stretchable Transparent Electrodes. *Nature* **2009**, *457*, 706–10.
9. Shen, T.; Gu, J. J.; Xu, M.; Wu, Y. Q.; Bolen, M. L.; Capano, M. A.; Engel, L. W.; Ye, P. D. Observation of Quantum-Hall Effect in Gated Epitaxial Graphene Grown on SiC (0001). *Appl. Phys. Lett.* **2009**, *95*, 172105.
10. Wu, X. S.; Hu, Y. K.; Ruan, M.; Madiomanana, N. K.; Hankinson, J.; Sprinkle, M.; Berger, C.; de Heer, W. A. Half Integer Quantum Hall Effect in High Mobility Single Layer Epitaxial Graphene. *Appl. Phys. Lett.* **2009**, *95*, 223108.
11. Meyer, J. C.; Geim, A. K.; Katsnelson, M. I.; Novoselov, K. S.; Booth, T. J.; Roth, S. The Structure of Suspended Graphene Sheets. *Nature* **2007**, *446*, 60–3.
12. Barone, V.; Hod, O.; Scuseria, G. E. Electronic Structure and Stability of Semiconducting Graphene Nanoribbons. *Nano Lett.* **2006**, *6*, 2748–54.
13. Han, M. Y.; Ozyilmaz, B.; Zhang, Y. B.; Kim, P. Energy Band-Gap Engineering of Graphene Nanoribbons. *Phys. Rev. Lett.* **2007**, *98*, 206805.
14. Wang, Z. F.; Shi, Q. W.; Li, Q. X.; Wang, X. P.; Hou, J. G.; Zheng, H. X.; Yao, Y.; Chen, J. Z-shaped Graphene Nanoribbon Quantum Dot Device. *Appl. Phys. Lett.* **2007**, *91*, 053109.
15. Zhang, Y.; Tang, T.-T.; Girit, C.; Hao, Z.; Martin, M. C.; Zettl, A.; Crommie, M. F.; Shen, Y. R.; Wang, F. Direct Observation of a Widely Tunable Bandgap in Bilayer Graphene. *Nature* **2009**, *459*, 820–3.
16. Kuzmenko, A. B.; Crassee, I.; van der Marel, D.; Blake, P.; Novoselov, K. S. Determination of the Gate-Tunable Band Gap and Tight-Binding Parameters in Bilayer Graphene Using Infrared Spectroscopy. *Phys. Rev. B.* **2009**, *80*, 165406.
17. Morozov, S. V.; Novoselov, K. S.; Katsnelson, M. I.; Schedin, F.; Elias, D. C.; Jaszczak, J. A.; Geim, A. K. Giant Intrinsic Carrier Mobilities in Graphene and Its Bilayer. *Phys. Rev. Lett.* **2008**, *100*, 016602.
18. Aoki, M.; Amawashi, H. Dependence of Band Structures on Stacking and Field in Layered Graphene. *Solid State Commun.* **2007**, *142*, 123–7.
19. Lu, C. L.; Chang, C. P.; Huang, Y. C.; Chen, R. B.; Lin, M. L. Influence of an Electric Field on the Optical Properties of Few-Layer Graphene with AB Stacking. *Phys. Rev. B.* **2006**, *73*, 144427.
20. Latil, S.; Henrard, L. Charge Carriers in Few-Layer Graphene Films. *Phys. Rev. Lett.* **2006**, *97*, 036803.
21. Grüneis, A.; Attaccalite, C.; Wirtz, L.; Shiozawa, H.; Saito, R.; Pichler, T.; Rubio, A. Tight-binding Description of the Quasiparticle Dispersion of Graphite and Few-Layer Graphene. *Phys. Rev. B.* **2008**, *78*, 205425.
22. Zhang, F.; Sahu, B.; Min, H.; MacDonald, A. H. Band Structure of ABC-Stacked Graphene Trilayers. *Phys. Rev. B.* **2010**, *82*, 035409.
23. Liu, Y. P.; Goolaup, S.; Murapaka, C.; Lew, W. S.; Wong, S. K. Effect of Magnetic Field on the Electronic Transport in Trilayer Graphene. *ACS Nano* **2010**, *4*, 7087–92.
24. Craciun, M. F.; Russo, S; Yamamoto, M; Oostinga, J. B.; Morpurgo, A. F.; Tarucha, S. Trilayer Graphene is a Semimetal with a Gate-Tunable Band Overlap. *Nat. Nanotechnol.* **2009**, *4*, 383–8.
25. Ni, Z. H.; Wang, Y. Y.; Yu, T.; Shen, Z. X. Raman Spectroscopy and Imaging of Graphene. *Nano Res.* **2008**, *1*, 273–91.
26. Ferrari, A. C.; Meyer, J. C.; Scardaci, V.; Casiraghi, C.; Lazzeri, M.; Mauri, F.; Piscanec, S.; Jiang, D.; Novoselov, K. S.; Roth, S.; et al. Raman Spectrum of Graphene and Graphene Layers. *Phys. Rev. Lett.* **2006**, *97*, 187401.
27. Ni, Z. H.; Wang, H. M.; Kasim, J.; Feng, H. Y. P.; Shen, Z. X. Graphene Thickness Determination Using Reflection and Contrast Spectroscopy. *Nano Lett.* **2007**, *7*, 2758–63.
28. Xuefeng, W.; Ming, Z.; Nolte, D. D. Optical Contrast and Clarity of Graphene on an Arbitrary Substrate. *Appl. Phys. Lett.* **2009**, *95*, 081102.
29. Malard, L. M.; Pimenta, M. A.; Dresselhaus, G.; Dresselhaus, M. S. Raman Spectroscopy in Graphene. *Phys. Rep.* **2009**, *473*, 51–87.
30. Calizo, I.; Bejenari, I.; Rahman, M.; Guanxiong, L.; Balandin, A. A. Ultraviolet Raman Microscopy of Single and Multilayer Graphene. *J. Appl. Phys.* **2009**, *106*, 043509.
31. Hao, Y. F.; Wang, Y. Y.; Wang, L.; Ni, Z. H.; Wang, Z. Q.; Wang, R.; Koo, C. K.; Shen, Z. X.; Thong, J. T. L. Probing Layer Number and Stacking Order of Few-Layer Graphene by Raman Spectroscopy. *Small* **2010**, *6*, 195–200.
32. Dong-Keun, K.; Dongchan, J.; Jae-Hyun, C.; Hu-Jong, L.; Kee-Su, P. Inelastic Scattering in a Monolayer Graphene Sheet: A Weak-Localization Study. *Phys. Rev. B* . **2008**, *78*, 125409.
33. Xin-Zhong, Y.; Ting, C. S. Weak Localization of Dirac Fermions in Graphene. *Phys. Rev. Lett.* **2008**, *101*, 126801.
34. McCann, E.; Kechedzhi, K.; Fal'ko, V. I.; Suzuura, H.; Ando, T.; Altshuler, B. L. Weak-Localization Magnetoresistance and Valley Symmetry in Graphene. *Phys. Rev. Lett.* **2006**, *97*, 146805.
35. Fal'ko, V. I.; Kechedzhi, K.; McCann, E.; Altshuler, B. L.; Suzuura, H.; Ando, T. Weak Localization in Graphene. *Solid State Commun.* **2007**, *143*, 33–8.
36. Tan, C.; Tan, Z.; Ma, L.; Qu, F.; Yang, F.; Chen, J.; Liu, G.; Yang, H.; Yang, C.; Lu, L. Observation of Electron Weak Localization and Correlation Effects in Disordered Graphene. *Sci. Chin., Ser. G* **2009**, *52*, 1293–8.
37. Moser, J.; Tao, H.; Roche, S.; Alzina, F.; Torres, C. M. S.; Bachtold, A. Magnetotransport in Disordered Graphene Exposed to Ozone: From Weak to Strong Localization. *Phys. Rev. B.* **2010**, *81*, 205445.
38. Eroms, J.; Weiss, D. Weak Localization and Transport Gap in Graphene Antidot Lattices. *New. J. Phys.* **2009**, *11*, 095021.
39. Krstić, V.; Obergfell, D.; Hansel, S.; Rikken, G. L. J. A.; Blokland, J. H.; Ferreira, M. S.; Roth, S. Graphene-Metal

Interface: Two-Terminal Resistance of Low-Mobility Graphene in High Magnetic Fields. *Nano Lett.* **2008**, *8*, 1700–3.
40. Khveshchenko, D. V. Magnetic-Field-Induced Insulating Behavior in Highly Oriented Pyrolitic Graphite. *Phys. Rev. Lett.* **2001**, *87*, 206401.
41. Zhang, Y.; Jiang, Z.; Small, J. P.; Purewal, M. S.; Tan, Y. W.; Fazlollahi, M.; Chudow, J. D.; Jaszczak, J. A.; Stormer, H. L.; Kim, P. Landau-Level Splitting in Graphene in High Magnetic Fields. *Phys. Rev. Lett.* **2006**, *96*, 136806.
42. Giesbers, A. J. M.; Ponomarenko, L. A.; Novoselov, K. S.; Geim, A. K.; Katsnelson, M. I.; Maan, J. C.; Zeitler, U. Gap Opening in the Zeroth Landau Level of Graphene. *Phys. Rev. B* . **2009**, *80*, 201403.
43. Cho, S.; Fuhrer, M. S. Charge Transport and Inhomogeneity Near the Minimum Conductivity Point in Graphene. *Phys. Rev. B.* **2008**, *77*, 81402.
44. Martin, J.; Akerman, N.; Ulbricht, G.; Lohmann, T.; Smet, J. H.; Von Klitzing, K.; Yacoby, A. Observation of Electron-Hole Puddles in Graphene Using a Scanning Single-Electron Transistor. *Nat. Phys.* **2008**, *4*, 144–148.
45. Hwang, E. H.; Adam, S.; Das Sarma, S. Carrier Transport in Two-Dimensional Graphene Layers. *Phys. Rev. Lett.* **2007**, *98*, 186806.
46. Hwang, E. H.; Das Sarma, S. Screening-Induced Temperature-Dependent Transport in Two-Dimensional Graphene. *Phys. Rev. B.* **2009**, *79*, 165404.
47. Hwang, E. H.; Das Sarma, S. Acoustic Phonon Scattering Limited Carrier Mobility in Two-Dimensional Extrinsic Graphene. *Phys. Rev. B.* **2008**, *77*, 115449.
48. Zhu, W.; Perebeinos, V.; Freitag, M.; Avouris, P. Carrier Scattering, Mobilities, and Electrostatic Potential in Monolayer, Bilayer, and Trilayer Graphene. *Phys. Rev. B* **2009**, *80*, 235402.
49. Abergel, D. S. L.; Apalkov, V.; Berashevich, J.; Ziegler, K.; Chakraborty, T. Properties of Graphene: A Theoretical Perspective. *Adv. Phys.* **2010**, *59*, 261–482.
50. Cheianov, V. V.; Fal'ko, V. I. Friedel Oscillations, Impurity Scattering, and Temperature Dependence of Resistivity in Graphene. *Phys. Rev. Lett.* **2006**, *97*, 226801.
51. Mak, K. F.; Shan, J.; Heinz, T. F. Electronic Structure of Few-Layer Graphene: Experimental Demonstration of Strong Dependence on Stacking Sequence. *Phys. Rev. Lett.* **2010**, *104*, 176404.
52. Otani, M.; Takagi, Y.; Koshino, M.; Okada, S. Phase Control of Magnetic State of Graphite Thin Films by Electric Field. *Appl. Phys. Lett.* **2010**, *96*, 242504.
53. Latil, S.; Henrard, L. Charge Carriers in Few-Layer Graphene Films. *Phys. Rev. Lett.* **2006**, *97*, 036803.
54. Avetisyan, A. A.; Partoens, B.; Peeters, F. M. Stacking Order Dependent Electric Field Tuning of the Band Gap in Graphene Multilayers. *Phys. Rev. B.* **2010**, *81*, 115432.
55. Avetisyan, A. A.; Partoens, B.; Peeters, F. M. Electric Field Tuning of the Band Gap in Graphene Multilayers. *Phys. Rev. B.* **2009**, *79*, 035421.
56. Lui, C. H.; Li, Z.; Chen, Z.; Klimov, P. V.; Brus, L. E.; Heinz, T. F. Imaging Stacking Order in Few-Layer Graphene. *Nano Lett.* **2010**, *11*, 164–9.
57. Chen, J.-H.; Jang, C.; Xiao, S.; Ishigami, M.; Fuhrer, M. S. Intrinsic and Extrinsic Performance Limits of Graphene Devices on $SiO_2$. *Nat. Nanotechnol.* **2008**, *3*, 206–9.